

# Characterization of the nontrivial and chaotic behavior that occurs in a simple city traffic model

J. Villalobos,<sup>1,2</sup> B. A. Toledo,<sup>3,a)</sup> D. Pastén,<sup>3</sup> V. Muñoz,<sup>3</sup> J. Rogan,<sup>3</sup> R. Zarama,<sup>1,2</sup> N. Lammoglia,<sup>1,2</sup> and J. A. Valdivia<sup>2,3</sup>

<sup>1</sup>*Departamento de Ingeniería Industrial, Universidad de los Andes, 110321 Bogotá, Colombia*

<sup>2</sup>*CEIBA Complejidad, 110321 Bogotá, Colombia*

<sup>3</sup>*Departamento de Física, Facultad de Ciencias, Universidad de Chile, 7800024 Santiago, Chile*

(Received 16 October 2009; accepted 14 January 2010; published online 4 March 2010)

We explore in detail the nontrivial and chaotic behavior of the traffic model proposed by Toledo *et al.* [Phys. Rev. E **70**, 016107 (2004)] due to the richness of behavior present in the model, in spite of the fact that it is a minimalistic representation of basic city traffic dynamics. The chaotic behavior, previously shown for a given lower bound in acceleration/brake ratio, is examined more carefully and the region in parameter space for which we observe this nontrivial behavior is found. This parameter region may be related to the high sensitivity of traffic flow that eventually leads to traffic jams. Approximate scaling laws are proposed. © 2010 American Institute of Physics. [doi:10.1063/1.3308597]

**Urban traffic is interesting not only due to its obvious social and economical impact, but also due to its complexity. It is not unusual for drivers to get stuck in a traffic jam that apparently emerged from nowhere. A situation like this is believed to emerge from a sudden change in the driving of some vehicle combined with the reaction time of neighboring drivers. In this way, a perturbation induced by some driver will back propagate through the system possibly affecting vehicles far away. In this article, we study the acceleration behavior of a given driver as one of the possible causes leading to a traffic jam. We based the present study on a previous work that showed theoretically the intrinsic chaotic nature of the traffic in cities, and we extend those results to a broader range of accelerations and deceleration ratios. In this way, our simulations suggest that high deceleration/acceleration ratios may be at the root of emergent traffic jams.**

## I. INTRODUCTION

The study of urban traffic from a physical viewpoint<sup>1–6</sup> has shown to be interesting not only due to its obvious social and economical<sup>7</sup> impact, but also due to its complexity,<sup>8,9</sup> which is experienced daily by drivers. This complex behavior has been studied from many perspectives, ranging from statistical and cellular automaton models to hydrodynamical and mean field approaches.<sup>10–13</sup> As a complex system, a traffic network may display emergent dynamics,<sup>10</sup> chaotic behavior,<sup>1,14–16</sup> self-organization,<sup>17</sup> etc.

In this work we deepen our understanding of the city traffic model proposed in Ref. 1, which displays nontrivial dynamics and chaos, due to the finite acceleration and braking capabilities of the vehicles for a set of parameters that is relevant for standard cities. We will discuss below that the ratio of the accelerating and braking capabilities will play a

crucial role in determining the size of the region in parameter space where the chaotic and nontrivial behavior can be observed. Furthermore, the nontrivial behavior in this model arises even in the nonchaotic region due to the existence of periodic trajectories that have multiple periods. We will show below that it is precisely this type of microscopic dynamics that cannot be observed in traditional cellular automaton and hydrodynamical models.

The appearance of chaos in such a minimal model of city traffic strongly suggests that chaotic behaviors should be at the root of many common complex macroscopic traffic states. To achieve our aim of characterizing the nontrivial dynamics and the chaotic behavior of the model we do two things: (a) we bound the region on which the nontrivial dynamics and the chaotic behavior occur, and (b) we compute a numerical Lyapunov exponent<sup>18</sup> of the system in parameter space. This behavior can then be understood in terms of approximate scaling relations, which we derive.

This paper is organized as follows. In Sec. II we recall briefly the model introduced in Ref. 1. In Sec. III we define the nontrivial region using the bifurcation points observed in the bifurcation diagrams. Some of these points can be found analytically, whereas others must be found numerically. We devote this section to the analysis of the period-one and period-two attractors that can be seen on the bifurcation diagrams of the model. In Sec. IV we analyze the behavior of the system through a numerical Lyapunov exponent for several sets of parameters and construct approximate scaling relations. Finally, Sec. V presents the conclusions to the paper. The specific details of the model are presented in the Appendix of the paper.

## II. MODEL

We follow the dynamics of one vehicle moving through a sequence of traffic lights in one dimension, as originally proposed in Ref. 1. A car in this sequence of traffic lights can have (a) an acceleration  $a_+$  until its velocity reaches the

<sup>a)</sup>Electronic mail: btoledo@macul.ciencias.uchile.cl.

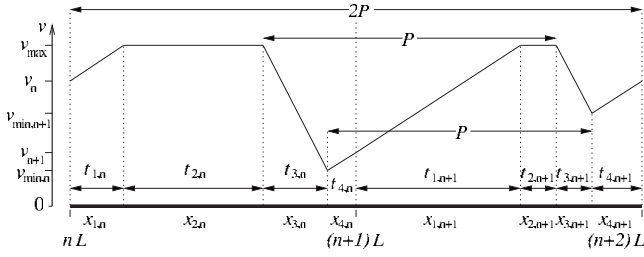


FIG. 1. Reference diagram for the dynamics of the car model. In this particular case we show a sequence of three traffic lights, where the velocity of the car at the light  $n$ , namely,  $v_n$ , is the same as the velocity at light  $n+2$ . The car has speed  $v_{n+1}$  at light  $n+1$ .

cruising speed  $v_{\max}$ , (b) a constant speed  $v_{\max}$  with zero acceleration, or (c) a negative acceleration  $-a_-$  until it stops. Therefore, we can summarize the equations of motion for the vehicle as

$$\frac{dv}{dt} = \begin{cases} a_+ \theta(v_{\max} - v), & \text{accelerate,} \\ -a_- \theta(v), & \text{brake,} \end{cases} \quad (1)$$

where  $\theta(x)$  is the Heaviside step function.

As the car approaches the  $n$ th traffic light with velocity  $v_{\max}$ , the driver must make a decision depending on the sign of  $\sin(\omega_n t + \phi_n)$  at the distance  $v_{\max}^2/2a_-$  (the last stopping point to arrive with null velocity at the traffic light). The frequency  $\omega_n$  and the phase  $\phi_n$  at the  $n$ th traffic light are used to control the traffic.

If  $\sin(\omega_n t + \phi_n) > 0$  (green light) the driver continues through the traffic light at speed  $v_{\max}$ . If  $\sin(\omega_n t + \phi_n) \leq 0$  (red light) the driver starts braking with  $-a_-$  until it reaches the traffic light with speed  $v=0$  and waits for the next green light, or until the light turns green again with  $v \neq 0$ , at which point it starts accelerating with  $a_+$  (see situation before the  $n$ th+1 traffic light in Fig. 1). We will choose parameters such that  $v_{\max}^2/2a_+ + v_{\max}^2/2a_- < L_n$ , so that  $v=v_{\max}$  before the decision point. Also in general it makes sense that the period  $2\pi/\omega_n > \text{Max}(v_{\max}/a_-, v_{\max}/a_+)$  so that the traffic light does not change too fast from green to red.

For the purpose of illustration, in this paper we will make the simplifying assumptions  $L_n=L$ ,  $\omega_n=\omega$ , and  $\phi_n=0$ . The situation of a green wave, which is defined by  $\phi_n = \phi_{n-1} - \omega L_n/v_{\text{wave}}$ , will give similar results from the bifurcation diagram to the resonant behavior, as demonstrated in Ref. 2. Hence, the assumptions taken above also represent qualitatively the trends of a more general situation with variable street length. In our model, at time  $t$  all lights are green if  $\sin(\omega t) > 0$  and red otherwise. Here  $\omega$  represents the frequency of the traffic lights. The car enters the sequence of traffic lights with velocity  $v_0$  at time  $t_0$ . The set of rules described above defines a two-dimensional (2D) map  $M(t_n, v_n)$  that evolves the state  $(t_n, v_n)$  at the  $n$ th traffic light to the state  $(t_{n+1}, v_{n+1})$  at the  $(n+1)$ th traffic light. This map is constructed explicitly in Ref. 1. The generic behavior of this model is depicted in Fig. 1.

For ease of handling we work with a normalized version of the model by defining a cruising time  $T_c=L/v_{\max}$ , a nor-

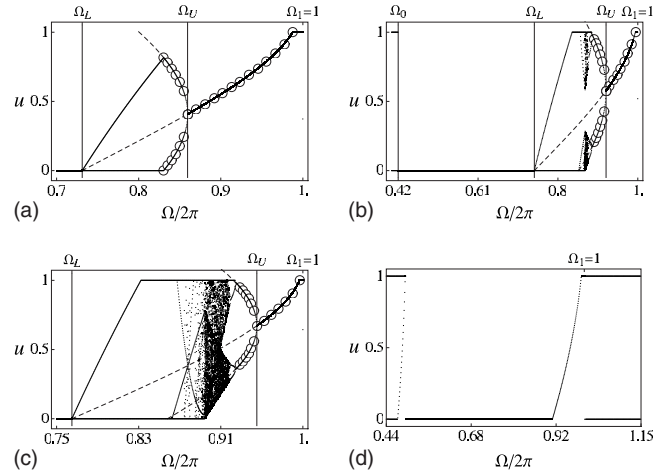


FIG. 2. Bifurcation diagrams for  $u=v/v_{\max}$  as a function of  $\Omega/2\pi$  for  $A_+ = 2a_o$  and different values of  $A_-$ . The region of the nontrivial dynamics and chaotic behavior bounded by  $\Omega_L < \Omega < \Omega_U$  is shown for (a)  $A_- = 4a_o$ , (b)  $A_- = 6a_o$ , and (c)  $A_- = 8a_o$ . The open circles correspond to the stable period-one and period-two orbits, while the dashed line to the unstable period-one and period-two orbits, which are derived analytically from Sec. III. Bifurcation diagram (d) shows the behavior of the model for  $A_+ = A_- = 10a_o$ . In (b) we have included  $\Omega_0$  for reference [see Eq. (4)].

malized speed  $u=v/v_{\max}$ , a normalized time  $\tau=t/T_c$ , and a normalized distance  $\bar{x}=x/L$ . With this normalization the evolution described by Eq. (1) can be written as

$$\frac{du}{d\tau} = \begin{cases} A_+ \theta(1 - u), & \text{accelerate,} \\ -A_- \theta(u), & \text{brake,} \end{cases} \quad (2)$$

where  $A_+ = a_+ L/v_{\max}^2$ ,  $A_- = a_- L/v_{\max}^2$ , and  $\Omega = \omega T_c$  is the normalized traffic light's frequency. The restrictions are now

$$A_+^{-1} + A_-^{-1} < 2, \quad \frac{\Omega}{2\pi} < \frac{1}{\text{Max}(A_+^{-1}, A_-^{-1})}, \quad (3)$$

so that  $v=v_{\max}$  ( $u=1$ ) before the decision point, and the traffic light does not change too fast from green to red. See the Appendix for a complete construction of the map. Some realistic city traffic parameters are, for example,  $L=200$  [m],  $v_{\max}=14$  [m/s],  $a_+=2$  [m/s<sup>2</sup>], and  $a_-=6$  [m/s<sup>2</sup>]. It will be useful to define the scaling variable  $a_o=L/v_{\max}^2 = 1.02041$  [s<sup>2</sup>/m] for the acceleration, so that for the case of  $A_+=2 \times 200/14^2 = 2a_o$  and  $A_-=6a_o$  we have the bifurcation diagram of Fig. 2(b), displaying the nontrivial dynamics and the chaotic behavior. It is important to mention that this type of behavior is not considered by other models. Indeed, this type of microscopic dynamics cannot be observed in traditional cellular automaton models and hydrodynamical models, where the transition from  $\Omega_L$  to  $\Omega_U$  in the bifurcation diagram is reduced to a single point, namely,  $\Omega_L = \Omega_U$ . Hence, the traditional models of city traffic miss an important part of this bifurcation diagram, which occurs for finite accelerating and braking capabilities of the car, as suggested in Refs. 1 and 2. Let us note that it is possible to construct the associated bifurcation diagram for the time variable  $\xi_n = \omega t_n \text{ mod } 2\pi$ , or  $\xi_n = \Omega \tau_n \text{ mod } 2\pi$  in normalized form, but we will characterize the bifurcations of the system through the bifurcation diagram for  $u_n = v_n/v_{\max}$ .

### III. BIFURCATION ANALYSIS

In this section we will characterize the region in parameter space defined by  $\Omega$ ,  $A_+$ , and  $A_-$ , where the nontrivial dynamics and the chaotic behavior occur in this model. From Fig. 2 we can observe that there is a transition at  $\Omega_1/2\pi = 1$  where the car goes through every traffic light without stopping, since the period of the traffic light  $2\pi/\omega$  is the same as the traveling time  $T_c$ . The critical behavior close to this transition point was studied in detail in Ref. 2. The region of interest, with respect to the parameter  $\Omega$ , where the nontrivial dynamics and chaotic behavior occur, is found between  $\Omega_L$  (lower bound) and  $\Omega_U$  (upper bound), as shown in Fig. 2. In Figs. 2(a)–2(c), we show the region in which the nontrivial dynamics and the chaotic behavior occur for three values of  $A_-$ . We note that variations in  $A_-$  change the size of the nontrivial region, and for some values the chaotic regime disappears, namely, Fig. 2(a). Now we will derive the analytical expressions for  $\Omega_L$  and  $\Omega_U$  as a function of  $A_+$  and  $A_-$ .

We first define the frequency  $\Omega_0$  where the car stops at every other traffic light, passing the light in between with  $v=v_{\max}$ . This means that the time between three lights must be equal to the time it takes to accelerate from  $v=0$  to  $v=v_{\max}$ , brake from  $v=v_{\max}$  to  $v=0$ , and travel at speed  $v=v_{\max}$  the remaining distance. If we call this time  $T_0$  (the time it takes to advance two lights), then

$$T_0 = \frac{v_{\max}}{a_+} + \frac{1}{v_{\max}} \left( 2L - \frac{v_{\max}^2}{2a_+} - \frac{v_{\max}^2}{2a_-} \right) + \frac{v_{\max}}{a_-}.$$

Since this time must be equal to the period of the traffic lights, we have

$$\frac{\Omega_0}{2\pi} = \left( \frac{1}{2A_+} + \frac{1}{2A_-} + 2 \right)^{-1}. \tag{4}$$

Let us calculate the lower bound  $\Omega_L$ . This is the frequency at which the car always stops, which means that the time between two lights must be equal to the time it takes to accelerate from  $v=0$  to  $v=v_{\max}$ , brake from  $v=v_{\max}$  to  $v=0$ , and travel at speed  $v=v_{\max}$  the remaining distance. If we call this time  $T_L$ , then

$$T_L = \frac{v_{\max}}{a_+} + \frac{1}{v_{\max}} \left( L - \frac{v_{\max}^2}{2a_+} - \frac{v_{\max}^2}{2a_-} \right) + \frac{v_{\max}}{a_-}.$$

Since this time must be equal to the period of the traffic lights, we have

$$\frac{\Omega_L}{2\pi} = \left( \frac{1}{2A_+} + \frac{1}{2A_-} + 1 \right)^{-1}. \tag{5}$$

Let us derive the upper bound  $\Omega_U$ . To the left of  $\Omega_U$  there is a period-two region ( $m=2$ ), at which the car goes through every other light with speeds  $0 < v_n, v_{n+1} < v_{\max}$ . We follow the notation described in Fig. 1 with  $v_{n+2}=v_n$ ,  $x_d=v_{\max}^2/2a_-$ , and the restrictions

$$x_{1,n} + x_{2,n} + x_{3,n} + x_{4,n} = L, \quad n = 1, 2. \tag{6}$$

For a period- $m$  orbit, we have

$$t_{4,n-1} + t_{1,n} + t_{2,n} + t_{3,n} = P, \tag{7}$$

where

$$\begin{aligned} x_{1,n} &= \frac{v_{\max}^2 - v_n^2}{2a_+} & t_{1,n} &= \frac{v_{\max} - v_n}{a_+}, \\ x_{2,n} &= L - x_{1,n} - x_d & t_{2,n} &= \frac{L - x_{1,n} - x_d}{v_{\max}}, \\ x_{3,n} &= \frac{v_{\max}^2 - v_{\min,n}^2}{2a_-} & t_{3,n} &= \frac{v_{\max} - v_{\min,n}}{a_-}, \\ x_{4,n} &= \frac{v_{n+1}^2 - v_{\min,n}^2}{2a_+} & t_{4,n} &= \frac{v_{n+1} - v_{\min,n}}{a_+}, \end{aligned}$$

with  $t_{4,n}=t_{4,n+m}$ ,  $v_{n+m}=v_n$ , and  $v_{\min,n}$ , as shown in Fig. 1, for the case  $m=2$ , which we now consider in detail. Note that Eq. (6) gives the solution

$$v_{\min,n+1} = \sqrt{\frac{a_-}{a_+ + a_-}} v_n.$$

By solving the remaining equations for the case  $m=2$ , we can obtain  $v_n(P)$  and  $v_{n+1}(P)$ , and in particular,  $P_U$  can be solved from  $v_n(P_U)=v_{n+1}(P_U)$ , which gives

$$P_U = \frac{L}{v_{\max}} + \frac{2a_+v_{\max}}{a_-(a_- + a_+)}$$

or

$$\frac{\Omega_U}{2\pi} = \left( \frac{2A_+}{A_-(A_+ + A_-)} + 1 \right)^{-1}. \tag{8}$$

It may be of interest to note the limit  $a_+=a_-$ , even though in city traffic  $a_- > a_+$ . Note that we could use this methodology to find any periodic orbit and the point it bifurcates. In Figs. 2(a)–2(c) we show the bifurcation diagram, which includes the region in which we have the nontrivial dynamics and the chaotic behavior, with these three relevant frequencies. Let us note that the range of parameters in Fig. 2 is relevant for real city traffic. For reference, we also show the stable and unstable period-one orbits, obtained from Eqs. (6) and (7), which agree with the numerical bifurcation diagram.

It is clear that Eqs. (5) and (8) give us a lower and upper bound for the region on which the nontrivial dynamics may occur in the model. Since  $\Omega_L \leq \Omega_U$ , we find that

$$A_- \geq A_+$$

for the nontrivial behavior to occur. Let us also note that given the form of Eqs. (5) and (8), it is sufficient to fix  $A_+$  and vary  $A_-/A_+$ . The chaotic region, which is contained in the region of the nontrivial dynamics, occurs for a larger ratio of  $A_-/A_+$ , as we will see below.

If we do not consider the finiteness of the acceleration and braking capabilities, then

$$\lim_{A_+, A_- \rightarrow \infty} \Omega_0 = \frac{1}{2},$$

$$\lim_{A_+, A_- \rightarrow \infty} \Omega_L = \Omega_1 = 1,$$

$$\lim_{A_+, A_- \rightarrow \infty} \Omega_U = \Omega_1 = 1,$$

which is exactly the statement we made above about the impossibility of observing the details of this nontrivial dynamics and chaotic behavior in traditional cellular automaton models and hydrodynamical models, where the transition from  $\Omega_L$  to  $\Omega_U$  to  $\Omega_1$  occurs at a single point, i.e.,  $\Omega_L = \Omega_U = \Omega_1$ . The way in which the system approaches this limit is shown in Fig. 2(d) for  $A_+ = A_- = 10a_o$ ; here the chaotic region disappears when  $\Omega_L \rightarrow \Omega_U$ . On the other hand, it is not difficult to show that the behavior that determines  $\Omega_0$  does appear in cellular automaton models.

Now that we have characterized the region in which we have the nontrivial behavior, we turn our attention to the chaotic region.

#### IV. ANALYSIS OF THE CHAOTIC REGION

We define the chaotic region as the region of the bifurcation diagram where we can estimate a positive numerical Lyapunov exponent (see below for a definition). The chaotic region is bounded by  $\Omega_L$  and  $\Omega_U \leq \Omega_1$  [see Eqs. (5) and (8)], but care must also be taken to satisfy the restrictions imposed by Eq. (3).

Let us note in Fig. 2(c) that as we reduce  $\Omega$ , the chaotic region stops when the attractor collides with the  $v=0$  threshold condition, which means that at some point the car must wait at the traffic light until the light turns green. Thus, the traffic light forces the system to go into periodic orbits, for a range of  $\Omega$ , which must go through the state  $(u=0, \Omega\tau \bmod 1=0)$ .

In order to compute a numerical Lyapunov exponent for the chaotic region, we follow Ref. 1. We take the initial condition  $t_0=0$  and  $v_0=0$ , and evolve the map for  $n_i=500$  iterations to reach the attractor. Once at the attractor, we numerically follow two trajectories slightly separated in velocity, that is,  $[\tau_n, u_n]$  and  $[\tau_n, u_n + \delta u_n]$ , with an initial velocity difference of  $\delta u_{n_i} = 10^{-5}$ . The separation of the trajectories behaves as

$$\delta_n = \delta_{n_i} e^{\lambda(n-n_i)}.$$

Hence, we can estimate the Lyapunov exponent  $\lambda$  by fitting a graph of  $\delta_n^2 = \delta\tau_n^2 + \delta u_n^2$  versus  $n-n_i$ , as shown in Fig. 3(a), for  $\Omega/2\pi=0.883$ ,  $A_- = 6.5a_o$ , and  $A_+ = 2a_o$ . Figures 3(b) and 3(c) show the bifurcation diagram and the numerical Lyapunov exponent as a function of  $\Omega$  for values of  $A_- = 6.5a_o$  and  $A_+ = 2a_o$ . Figure 3(b) is a bifurcation diagram for these values and has + marks above the  $\Omega/2\pi$  values for which it is positive. We choose the numerical threshold condition  $\lambda > 0.1$  to include a particular evolution in the chaotic region. This value, which defines a positive numerical Lyapunov exponent, is about the error in  $\lambda$  obtained in Fig. 3(a). Figure 3(c) has the value of  $\lambda$  in the same horizontal scale as the bifurcation diagram of Fig. 3(b). For  $\Omega$  values below the chaotic regime the two trajectories essentially converge to the same solution, and hence the Lyapunov exponents become  $\lambda \rightarrow -\infty$ .

Now that we have a procedure that allows us to estimate  $\lambda$ , we can look in parameter space the regions in which we

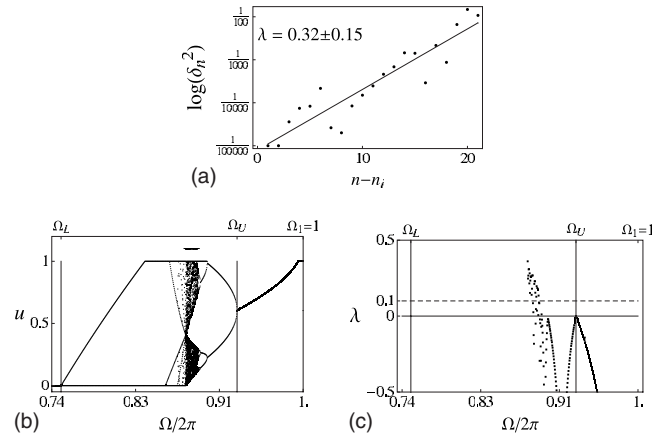


FIG. 3. (a)  $\log(\delta_n^2)$  vs  $n-n_i$  for  $\Omega/2\pi=0.883$ ,  $A_- = 6.5a_o$ , and  $A_+ = 2a_o$ ; points represent the simulation results, the solid line is the fit for the numerical Lyapunov exponent. (b) Bifurcation diagram for  $A_+ = 2a_o$  and  $A_- = 6.5a_o$ . The marks above the diagram are the values of  $\Omega/2\pi$  for which the numerical Lyapunov exponent is positive. (c) The numerical Lyapunov exponent as a function of  $\Omega$  for the bifurcation diagram in (b). The dashed line indicates the threshold we define to consider a positive numerical Lyapunov exponent, namely,  $\lambda > 0.1$ .

have  $\lambda > 0.1$ . In Figs. 4(a)–4(c) we plot the region of positive Lyapunov exponent in the  $A_+ - \Omega/2\pi$  space for  $A_- = 4a_o$ ,  $6a_o$ , and  $8a_o$ . In all figures the solid lines display the curves defined by  $\Omega_L$  and  $\Omega_U$ , and the restrictions given by Eq. (3) are satisfied. We note that as we increase the braking capability  $a_-$  we increase the size of the chaotic region in parameter space, as suggested in Ref. 1.

It is interesting to note that we need a braking capability  $a_-$  much larger than the accelerating capability  $a_+$  to obtain chaos. The relation seems to be  $a_- > 3a_+$  for chaos to appear. It is not possible to obtain a chaotic behavior for  $a_+ \sim a_-$ .

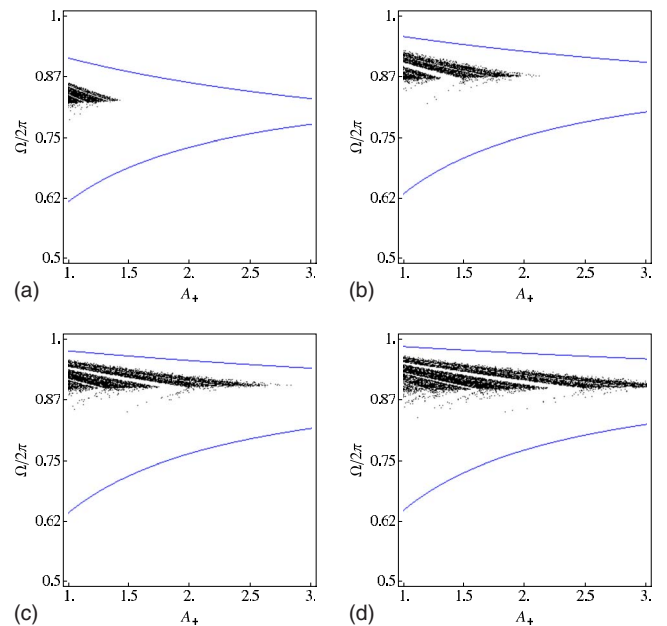


FIG. 4. (Color online) Chaotic regions for  $\Omega/2\pi$  vs  $A_+$  for (a)  $A_- = 4a_o$ , (b)  $A_- = 6a_o$ , (c)  $A_- = 8a_o$ , and (d)  $A_- = 10a_o$ . Black dots on the plots mean a positive numerical Lyapunov exponent. On all plots the solid lines represent  $\Omega_L$  and  $\Omega_U$ , see Eqs. (5) and (8), respectively. The restrictions given by Eq. (3) are satisfied.

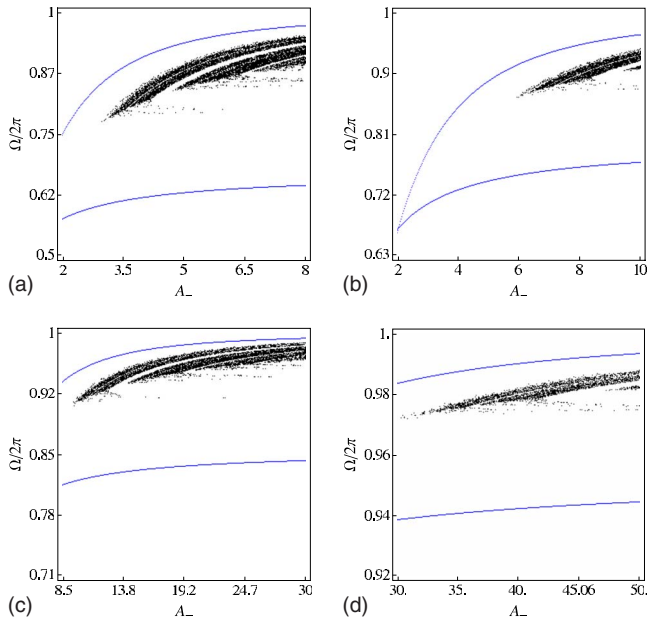


FIG. 5. (Color online) Chaotic regions for  $\Omega/2\pi$  vs  $A_+$  for (a)  $A_- = 1a_0$ , (b)  $A_- = 2a_0$ , (c)  $A_- = 3a_0$ , and (d)  $A_- = 10a_0$ . A black dot on the plots means a positive numerical Lyapunov exponent. On all plots the solid lines represent  $\Omega_L$  and  $\Omega_U$ , see Eqs. (5) and (8), respectively. The restrictions given by Eq. (3) are also included.

This is a result of interest in itself, which may have implications for city traffic. Notice that there are some regions of order, periodic windows, inside the chaotic region, and they run diagonally. We note that Figs. 4(a)–4(d) are strikingly similar, and there may be a way to map the three-dimensional parameter space into a 2D effective parameter space through some scaling relations. These scaling relations, which we will describe below, will show that chaos indeed appears if  $A_- \geq 3A_+$ , which corresponds to a relevant situation for real city traffic.

Similarly, we can fix  $A_+$  and look at the chaotic region in the  $A_-$  versus  $\Omega/2\pi$  parameter space, as shown in Figs. 5(a)–5(d). It is interesting to note that although we have fixed  $A_+$  the region for which we observe a positive numerical Lyapunov exponent only happens for a small region of values for  $\Omega$ . Our previous statement about the relation between  $A_+$  and  $A_-$  to obtain a chaotic behavior becomes more apparent. Again we observe that Figs. 5(a)–5(d) are strikingly similar, and it becomes more apparent that there may be a way to map the three-dimensional parameter space into a 2D effective parameter space through scaling relations.

Finally we fix  $\Omega$  and do an exploration of the  $A_- - A_+$  space. The results are shown in Fig. 6. As previously mentioned, we need a braking capability  $a_-$  larger than the accelerating capability  $a_+$  to obtain chaos, and notice that it is not possible to obtain a chaotic behavior for  $a_+ \sim a_-$ . Some regions of order inside the chaotic region can also be observed, and they run diagonally up to some point. A new feature appears however. If we look to the right side of these figures we observe that the dense region where we have a positive numerical Lyapunov exponent, which runs diagonally, starts to thin out for bigger values of  $A_-$ , while the regions of order stop going diagonally. They widen and start running horizon-

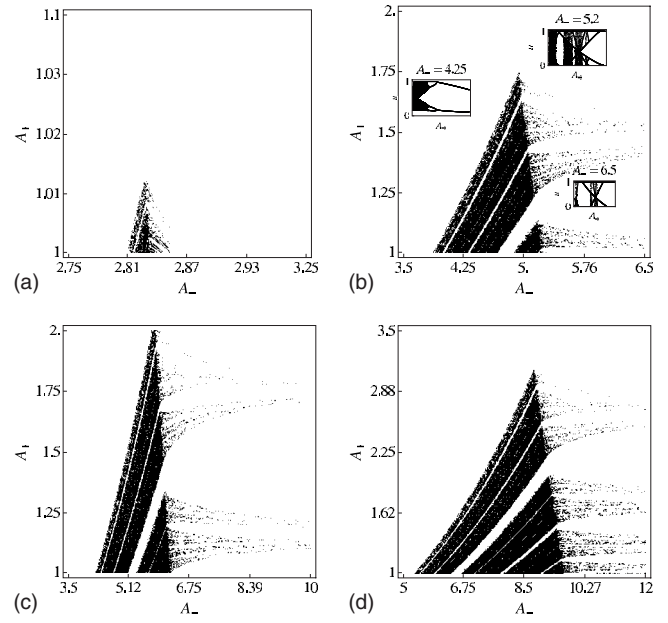


FIG. 6. Chaotic region in the  $A_- - A_+$  space for (a)  $\Omega/2\pi = 0.77$ , (b)  $\Omega/2\pi = 0.85$ , (c)  $\Omega/2\pi = 0.87$ , and (d)  $\Omega/2\pi = 0.91$ .

tally. This is an effect that takes place when the system is moving toward the limit  $a_- \rightarrow \infty$  ( $\Omega_U \rightarrow \Omega_1$ ) with constant  $a_+$ , which may be relevant in city traffic, and which is completely consistent with our previous observations. In Fig. 6(b) three insets have been added, corresponding to the bifurcation diagrams for  $u_n$  versus  $A_+$  with constant  $A_-$ . In the plot for  $A_- = 4.25$  we see that the chaotic region appears to the left of a period doubling cascade. Whereas in the diagram for  $A_- = 6.5$  this is not the case, and we observe a more complicated behavior. This behavior, which is also present in Fig. 2(c), occurs when the chaotic attractor collides with the  $u=0$  threshold around  $\Omega/2\pi \approx 0.9$ . It has to do with situations in which the car stops completely at a traffic light, and then needs to wait a while until the next green light. This complex dynamics gives rise to a behavior described by supertracks,<sup>19</sup> which will be studied in detail elsewhere.

### A. Approximate scaling

It is possible to capture some of the dynamics that we have previously discussed by doing an approximate rescaling of the axis in Figs. 4–6. From Fig. 4 it becomes apparent that we need to divide  $A_-$  by  $A_+$ , as originally suggested in Ref. 1, but that requires rescaling  $\Omega$  in some way. Hence, using the definitions of  $\Omega_L$  and  $\Omega_U$ , it becomes natural to rescale  $\Omega$  with

$$\Omega' = \frac{\Omega - \Omega_L(A_-)}{\Omega_U(A_-) - \Omega_L(A_-)}.$$

This rescaling is also suggested by the similar curvatures of the chaotic region and  $\Omega_U$  and  $\Omega_L$  in Figs. 4 and 5. With these two scaling laws, we can represent Figs. 4 and 5 by the single plot of Fig. 7(a). Let us note that besides the chaotic region, the periodic windows are clearly apparent. Hence, these approximate scaling laws allow us to approximate the 2D parameter space that describes the chaotic and nontrivial

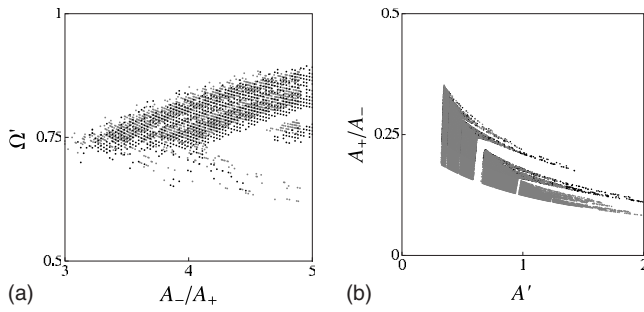


FIG. 7. Approximate scaling for (a)  $\Omega'$  vs  $A_-/A_+$ ; black values represent the data from Fig. 5(c); gray ones from Fig. 5(d). (b)  $A_+/A_-$  vs  $A'$ ; black values represent the data from Fig. 6(c); gray ones from Fig. 6(d).

behavior of the system. Here it becomes clear that the chaotic behavior can only occur for  $a_- \geq 3a_+$ , which is a realistic condition for today's cars.

It then remains to consider a way to scale the four panels represented in Fig. 6 into a single plot. It is natural to normalize the horizontal axis by

$$A' = \frac{A_- - A_u(\Omega, A_+)}{A_u(\Omega, A_+)}$$

and keep the vertical one as  $A_+/A_-$ . Here we have used

$A_u(\Omega, A_+)$

$$= \frac{A_+ \left( 1 - \frac{\Omega}{2\pi} \right) + \sqrt{A_+} \sqrt{\frac{\Omega}{2\pi} - 1} \sqrt{A_+ \frac{\Omega}{2\pi} - A_+ - 8 \frac{\Omega}{2\pi}}}{2 \left( \frac{\Omega}{2\pi} - 1 \right)},$$

which represents the  $A_-$  value evaluated from the definition of  $\Omega_U$ , namely, Eq. (8). Note that it does not make any sense to use the definition  $\Omega_L$  to rescale. Figure 7(b) is constructed with all the data from Figs. 6(c) and 6(d). This figure is even more striking than Fig. 7(a), for the periodic windows are better defined. It may also happen that this figure may be a fractal as we increase  $A'$ , which we plan to analyze elsewhere.

## V. CONCLUSIONS

We derived bounds for the nontrivial dynamics and chaotic behavior for the simple city traffic model previously presented in Refs. 1 and 2. The relevance of this study resides in that the range of parameters defined by these bounds is of relevance in city traffic, and is usually not considered in standard models of city traffic dynamics, such as cellular automata or hydrodynamic models.

We found that chaos is only possible if  $A_- \geq 3A_+$ , and that the chaotic region in the bifurcation diagram with respect to  $\Omega$  gets bigger as we increase this ratio. Note that this is a common situation on every day traffic since most cars have a braking capability (loose speed) larger than their acceleration capability. Hence, the dynamics of the system may be more prone to form an emergent traffic jam. It is interesting to note that this is exactly the tendency shown by drivers in crowded roads, where the usual car movement starts with a low acceleration ( $A_+$ ) and ends with a larger braking value

( $A_-$ ). Even though the analysis of the present paper is conducted on a simple model of one car in a sequence of traffic signals, it may be expected that this stop and go behavior in a dense city traffic may enhance the probability of producing a disordered state, and hence a traffic jam, which is, in this manner, a self-organized state.

Through a numerical exploration of the parameter space of the model, we found the combination of parameters for which the system shows a positive numerical Lyapunov exponent. We also found that the region of values of  $\Omega$  for which this occurs is small and has embedded on it windows of nonchaotic dynamics as expected, hinting at the possibility of controlling this nontrivial dynamics and chaotic behavior via the traffic light frequency. However, we also conclude that even for high values of  $A_-$  there are values of  $\Omega$  for which there is a positive numerical Lyapunov exponent, although not produced by a period doubling cascade, but by the discontinuities in this simple traffic model. Regarding a real life situation these observations highlight the fact that chaotic behavior may be present on city traffic systems regardless of driver behavior, arising from the traffic light existence itself.

## ACKNOWLEDGMENTS

This project has been financially supported by FONDECYT under Contract Nos. 1070854 (J.A.V.), 1080658 (V.M.), 1090225, and 1071062 (J.R.). B.A.T. acknowledges the financial support from a postdoctoral fellowship of the Departamento de Física of the Facultad de Ciencias of the Universidad de Chile. We also acknowledge COLCIENCIAS's financial support (J.V.), CEIBA'S financial support (J.V. and R.Z.), and the Research Fund of the Engineering Faculty of the Universidad de los Andes, Colombia (R.Z.). D.P. acknowledges the financial support from CONICYT doctoral fellowship (Grant No. 21070671).

## APPENDIX: THE $M(t, v)$ MAP

It is convenient to construct an exact map that relates successive crossings of the traffic lights. Let  $L$  be the distance between origin  $O$  and next traffic light. After crossing the  $n$ th light, the car reaches  $v_{\max}$  at

$$x_c = \frac{v_{\max}^2 - v_n^2}{2a_+} \rightarrow y_c = \frac{1}{2A_+} (1 - u_n^2),$$

$$t_c = t_n + \frac{v_{\max} - v_n}{a_+} \rightarrow \tau_c = \tau_n + \frac{1}{A_+} (1 - u_n),$$

$$v_c = v_{\max} \rightarrow u_c = 1,$$

and continues to move at constant velocity until the decision point

$$x_d = L_n - \frac{v_{\max}^2}{2a_-} \rightarrow y_d = 1 - \frac{1}{2A_-},$$

$$t_d = t_c + \frac{x_d - x_c}{v_{\max}} \rightarrow \tau_d = \tau_c + (y_d - y_c),$$

$$v_d = v_{\max} \rightarrow u_d = 1.$$

At this point we have two choices depending on the sign of  $\sin(\omega_n t_d + \phi_n)$ .

If  $\sin(\omega_n t_d + \phi_n) = \sin(\Omega \tau_d + \phi_n) > 0$ , the car reaches the traffic light with a state

$$x_{n+1} = L_n \rightarrow y_{n+1} = 1,$$

$$t_{n+1} = t_d + \frac{L_n - x_d}{v_{\max}} \rightarrow \tau_{n+1} = \tau_d + 1 - y_d,$$

$$v_{n+1} = v_{\max} \rightarrow u_{n+1} = 1.$$

If  $\sin(\omega_n t_d + \phi_n) = \sin(\Omega \tau_d + \phi_n) < 0$ , the car must start slowing down with  $a_-$ , and it will take an extra time  $\Delta t = v_{\max}/a_-$ , or  $\Delta \tau = 1/A_-$ , to reach the  $(n+1)$ th traffic light and stop. This time must be compared with the next time the light turns green  $t_g$ , at which point the car can accelerate again. Defining the phase  $\xi_d = \omega_n t_d + \phi_n = \Omega \tau_d + \phi_n$ , we can compute

$$\xi_g = \omega_n t_g + \phi_n = 2\pi \left( \text{Int} \left[ \frac{\xi_d}{2\pi} \right] + 1 \right),$$

where  $\text{Int}[x]$  is the integer part of  $x$ . Therefore, if  $t_d + \Delta t < t_g$ , or  $\tau_d + \Delta \tau < \tau_g$ , the car will cross the  $(n+1)$ th traffic light with

$$x_{n+1} = L_n \rightarrow y_{n+1} = 1,$$

$$t_{n+1} = t_g \rightarrow \tau_{n+1} = \tau_g,$$

$$v_{n+1} = 0 \rightarrow u_{n+1} = 0.$$

In the other case,  $t_d + \Delta t > t_g$ , or  $\tau_d + \Delta \tau > \tau_g$ , the car starts accelerating at the state

$$\begin{aligned} x_g &= x_d + v_d(t_g - t_d) - a_-(t_g - t_d)^2/2 \\ &\rightarrow y_g = y_d + u_d(\tau_g - \tau_d) - A_-(\tau_g - \tau_d)^2/2, \end{aligned}$$

$$t_g = t_g \rightarrow \tau_g = \tau_g,$$

$$v_g = v_d - a_-(t_g - t_d) \rightarrow u_g = u_d - A_-(\tau_g - \tau_d),$$

and again we have two cases before it reaches  $L$ . We need to determine if the car reaches  $v_{\max}$  before the light. We compute the distance at which the car reaches  $v_{\max}$ , namely,  $x_m = x_g + (v_{\max}^2 - v_g^2)/2a_+$ , or  $y_m = y_g + (1 - u_g^2)/2A_+$ . Therefore, if  $x_m > L$ , then the car reaches the traffic light with

$$x_{n+1} = L_n \rightarrow y_{n+1} = 1,$$

$$t_{n+1} = t_g + \frac{v_{n+1} - v_g}{a_+} \rightarrow \tau_{n+1} = \tau_g + \frac{1}{A_+}(u_{n+1} - u_g),$$

$$v_{n+1} = \sqrt{v_g^2 + 2a_+(L_n - x_g)} \rightarrow u_{n+1} = \sqrt{u_g^2 + 2A_+(1 - y_g)},$$

otherwise, it reaches  $v_{\max}$  at

$$x_m = x_m \rightarrow y_m = y_m,$$

$$t_m = t_g + \frac{v_{\max} - v_g}{a_+} \rightarrow \tau_m = \tau_g + \frac{1}{A_+}(1 - u_g),$$

$$v_m = v_{\max} \rightarrow u_f = 1,$$

and the light at

$$x_{n+1} = L_n \rightarrow y_{n+1} = 1,$$

$$t_{n+1} = t_m + \frac{L_n - x_m}{v_{\max}} \rightarrow \tau_{n+1} = \tau_m + (1 - y_m),$$

$$v_{n+1} = v_{\max} \rightarrow u_{n+1} = 1.$$

- <sup>1</sup>B. A. Toledo, V. Muñoz, J. Rogan, C. Tenreiro, and J. A. Valdivia, *Phys. Rev. E* **70**, 016107 (2004).
- <sup>2</sup>B. A. Toledo, E. Cerda, J. Rogan, V. Muñoz, C. Tenreiro, R. Zarama, and J. A. Valdivia, *Phys. Rev. E* **75**, 026108 (2007).
- <sup>3</sup>L. A. Wastavino, B. A. Toledo, J. Rogan, R. Zarama, V. Muñoz, and J. A. Valdivia, *Physica A* **381**, 411 (2007).
- <sup>4</sup>T. Nagatani, *Rep. Prog. Phys.* **65**, 1331 (2002).
- <sup>5</sup>T. Nagatani, *Physica A* **377**, 651 (2007).
- <sup>6</sup>S. Lämmer and D. Helbing, *J. Stat. Mech.: Theory Exp.* **2008**, P04019.
- <sup>7</sup>D. Helbing and M. Treiber, *Science* **282**, 2001 (1998).
- <sup>8</sup>Y. Bar-Yam, *Dynamics of Complex Systems* (Addison-Wesley, Reading, 1997).
- <sup>9</sup>G. Nicolis and I. Prigogine, *Exploring Complexity: An Introduction* (Freeman, San Francisco, 1989).
- <sup>10</sup>H. K. Lee, R. Barlovic, M. Schreckenberg, and D. Kim, *Phys. Rev. Lett.* **92**, 238702 (2004).
- <sup>11</sup>J. Matsukidaira and K. Nishinari, *Phys. Rev. Lett.* **90**, 088701 (2003).
- <sup>12</sup>N. Mitarai and H. Nakanishi, *Phys. Rev. Lett.* **85**, 1766 (2000).
- <sup>13</sup>K. Nishinari, M. Treiber, and D. Helbing, *Phys. Rev. E* **68**, 067101 (2003).
- <sup>14</sup>L. A. Safonov, E. Tomer, V. V. Strygin, Y. Ashkenazy, and S. Havlin, *Chaos* **12**, 1006 (2002).
- <sup>15</sup>S. Jamison and M. McCartney, *Chaos* **17**, 033116 (2007).
- <sup>16</sup>M. McCartney, *Physica A* **14**, 233 (2009).
- <sup>17</sup>S. Tadaki and M. Kikuchi, *Phys. Rev. E* **50**, 4564 (1994).
- <sup>18</sup>G. Boffetta, M. Cencini, M. Falcioni, and A. Vulpiani, *Phys. Rep.* **356**, 367 (2002).
- <sup>19</sup>E. M. Oblow, *Phys. Lett. A* **128**, 406 (1988).